NMR in Biomedicine

WILEY

NMR IN BIOMEDICINE

RESEARCH ARTICLE

Therapeutic Effects Assessment in Acute Lung Injury Using Hyperpolarized ^{129}Xe Magnetic Resonance

Yu Zheng[1] | Haidong Li[1,2] | Ming Zhang[1,2] | Xiaoling Liu[1,2] | Hongchuang Li[1,2] | Mingyan Yu[1,2] | Wenjie Wang[1,2] | Jiawei Zhu[1] | Xiuchao Zhao[1,2] | Haofeng Li[1,2] | Siya Wei[1] | Yeqing Han[1,2] | Xin Zhou[1,2,3]

[1]State Key Laboratory of Magnetic Resonance Spectroscopy and Imaging, National Center for Magnetic Resonance in Wuhan, Wuhan Institute of Physics and Mathematics, Innovation Academy for Precision Measurement Science and Technology, Chinese Academy of Sciences-Wuhan National Laboratory for Optoelectronics, Huazhong University of Science and Technology, Wuhan, China | [2]University of Chinese Academy of Sciences, Beijing, China | [3]School of Biomedical Engineering, Hainan University, Haikou, China

Correspondence: Xin Zhou (xinzhou@wipm.ac.cn)

Received: 28 July 2025 | **Revised:** 11 February 2026 | **Accepted:** 13 February 2026

Keywords: ^{129}Xe MR | acute lung injury | dexamethasone | gas exchange | treatment monitoring

ABSTRACT

Therapeutic effects in acute lung injury (ALI) vary considerably among individuals, presenting a significant clinical challenge in optimizing treatment strategies—particularly with agents such as glucocorticoids. Non-invasive techniques capable of quantifying pulmonary physiological changes in the lung are essential for evaluating treatment efficacy and elucidating underlying mechanisms. Herein, we investigated the feasibility of hyperpolarized ^{129}Xe magnetic resonance (MR) for assessing the effects of dexamethasone treatment in a rat model of ALI. Fifteen Wistar rats were randomly assigned to three groups ($n = 5$ each): a treatment group with lipopolysaccharide (LPS)-induced ALI treated with dexamethasone (DEX), an ALI group subjected to the same LPS induction but treated with normal saline, and a control group receiving only normal saline. All rats underwent ^{129}Xe MR, pulmonary function tests (PFTs), computed tomography (CT), and histological analysis. Quantitative results from ^{129}Xe MR were analyzed using Kruskal–Wallis tests followed by Conover–Iman multiple comparison tests. Correlations among MRI, PFTs, and CT findings were evaluated. The ratio of ^{129}Xe signal in red blood cells to pulmonary Membrane (RBC/Mem) was reduced in the ALI group compared with the control group (median, 0.356 [IQR,0.035] vs. 0.607 [IQR,0.086], $p < 0.001$) and partially recovered in the treatment group ($p < 0.001$). Notably, persistent functional impairment in the treatment group was not detected by PFTs or CT imaging. The RBC/Mem correlated well with forced vital capacity (FVC) and mean lung density (MLD) (both $p < 0.05$). Additionally, hematocrit (Hct) increased in the treatment group compared to the ALI group (Hct: median, 0.242 [IQR, 0.031] vs. 0.216 [IQR, 0.019], $p < 0.001$). These findings demonstrate the potential of hyperpolarized ^{129}Xe MR as a non-invasive and highly sensitive modality for detecting subtle or residual gas-exchange abnormalities, supporting its further application in interventional studies of acute lung injury.

Abbreviations: ALI, acute lung injury; ARDS, acute respiratory distress syndrome; CSSR, chemical shift saturation recovery; CT, computed tomography; DEX, dexamethasone sodium phosphate; FVC, forced vital capacity; Hct, hematocrit; LPS, lipopolysaccharide; Mem, membrane tissue; MLD, mean lung density; MRI, magnetic resonance imaging; MRS, MR spectroscopy; PFTs, pulmonary function tests; RBC, red blood cell; δ, the air-capillary barrier thickness; ω_{RBC}, ^{129}Xe chemical shift in RBC.

Yu Zheng, Haidong Li, and Ming Zhang contributed equally to this work.

1 | Introduction

Acute lung injury (ALI) is a disorder of acute inflammation that causes disruption of the lung endothelial and epithelial barriers. Its more severe form, acute respiratory distress syndrome (ARDS), which are characterized by the sudden onset of pulmonary infiltrates and impaired oxygenation, resulting from either pulmonary (direct) factors, such as biological, chemical, and physical hazards, or extrapulmonary (indirect) [1], for example, sepsis. ARDS has long posed a significant healthcare challenge, with an annual incidence of approximately 75 cases per 100,000 population and a mortality rate ranging from 27% to 45% [2, 3]. Moreover, there are currently no clinically approved medications that can effectively reduce mortality in ARDS patients [4]. The management of this condition largely depends on supportive care [2]. Corticosteroids have attracted considerable clinical interest for their ability to mitigate pulmonary and systemic injury in ALI/ARDS patients [5], owing to their potent anti-inflammatory and antifibrotic effects. Recent meta-analyses suggest that glucocorticoids therapy can significantly improve oxygenation [6]. However, prolonged systemic glucocorticoids therapy may also lead to complications such as hypertension and other adverse effects [7]. Therefore, careful monitoring of therapeutic efficacy and prudent administration of medication are essential across the broad phenotypic spectrum of ALI/ARDS patients.

ALI/ARDS is characterized by severe impairment of gas exchange with a decrease in arterial oxygen partial pressure (PaO_2) and/or reduced oxygen utilization. Numerous strategies have been implemented to monitor respiratory status and treatment responses in ALI. The ratio of PaO_2 to the fraction of inspired oxygen (FiO_2) remains a standard metric for assessing the severity of ALI/ARDS [8]. However, PaO_2 measurement requires invasive arterial blood sampling, which may be contraindicated in patients prone to bleeding, like patients with coagulation dysfunction or individuals treated with anticoagulant drugs. Computed tomography (CT) offers detailed assessment of lung aeration and edema [9, 10], but the associated ionizing radiation limits routine clinical use. Lung ultrasound (LUS) has emerged as a bedside tool for monitoring lung impairment. Previous studies have demonstrated strong correlations between LUS reaeration score and improvements in PaO_2 following interventions such as positive end-expiratory pressure (PEEP) application [11–13]. Nevertheless, ultrasound predominantly visualizes subpleural lung areas and may be limited in cases of subcutaneous emphysema or diffuse edema [14]. Therefore, non-invasive, sensitive methods for assessing lung function are needed to assess treatment response in patients with ALI/ARDS [15].

Hyperpolarized (HP) ^{129}Xe magnetic resonance imaging (MRI) is a promising imaging modality for non-invasive, radiation-free assessment of pulmonary function [16–18] and microstructure [19–21]. Upon inhalation, xenon gas rapidly diffuses through the airways into the alveolar spaces, permeates the blood-gas barrier, and dissolves into tissues, plasma, and red blood cells (RBCs) [22]. The dissolved-phase ^{129}Xe exhibits distinct chemical shifts at approximately 197 ppm in pulmonary tissues and plasma (membrane tissue) and around 218 ppm in RBCs of humans, with a slightly lower value observed in rats (~210 ppm), relative to the gas-phase signal. This property allows ^{129}Xe MR to assess pulmonary function [23, 24]. HP ^{129}Xe MR has been successfully utilized for the assessment of various diseases, including COPD [25–28], cystic fibrosis (CF) [29–31], asthma [32], and pulmonary hypertension [33, 34].

Recent studies have shown that HP ^{129}Xe MR can sensitively detect post-treatment changes in various pulmonary diseases. In COPD, it identified impaired gas exchange in newly ventilated regions following bronchodilator therapy [35]. In idiopathic pulmonary fibrosis (IPF) [36], patients who received 1 year of antifibrotic therapy demonstrated an increase in the RBC-to-Mem ratio relative to baseline values, a change that was not detectable by conventional pulmonary function tests (PFTs) (forced vital capacity [FVC] and diffusing capacity of the lung for carbon monoxide [DL_{CO}]). Similarly, in pulmonary hypertension, ^{129}Xe MR detected improved RBC transfer even at low serum drug levels during long-term therapy [37]. While most studies focus on chronic lung diseases, few have explored this technology in acute, heterogeneous conditions like ALI. Nevertheless, prior work has demonstrated the sensitivity of RBC/Mem measurements in tracking gas exchange changes in LPS-induced ALI models [38, 39] and lung lesions induced by bleomycin [40]. Animal models remain critical for studying disease mechanisms and predicting therapeutic outcomes [41, 42].

In this study, we investigated the feasibility of using hyperpolarized ^{129}Xe MR to quantify pulmonary physiological changes following glucocorticoid treatment in a rat model of ALI. All animals underwent hyperpolarized ^{129}Xe MR, PFTs, CT, and histopathological analysis. Quantitative parameters derived from ^{129}Xe MR were compared among groups, and their correlations with conventional assessment methods were evaluated to determine the potential clinical utility of this imaging modality.

2 | Methods

2.1 | ^{129}Xe Polarization and Delivery

Isotopically enriched xenon gas (86% ^{129}Xe) was polarized using a commercial polarizer (verImagin Healthcare, Wuhan, China) operating in a continuous mode. The available polarization of xenon gas within the Tedlar bag was approximately 40%. Polarized xenon gas was administered to the rats through a home-built, MR-compatible gas delivery system, controlled by a homemade *LabVIEW* program [43]. During MR examinations, the rat was ventilated with xenon and oxygen gas alternately, while the airway pressure in the lungs was continuously monitored in real time.

2.2 | Animal Preparation

All the animal experimental protocols were approved by the institutional animal care committee. Anesthesia was induced with 5% isoflurane (RWD Life Science, Shenzhen, China) in air and maintained at 2% during procedures. Lipopolysaccharide (LPS; 4 mg/mL, Sigma, USA) and dexamethasone sodium phosphate (DEX; 2 mg/mL, MedChemExpress, Shanghai, China) [44], both dissolved in normal saline (NS), were used to induce and treat ALI rat model, respectively. After 1 week of

acclimatization, 15 male Wistar rats (7 weeks old, 230–260 g) were randomly divided into three groups ($n = 5$ per group): a control group receiving only NS, a group with LPS-induced lung injury then treated with normal saline (ALI group), and a group with LPS-induced lung injury then treated with DEX (treatment group). (Figure 1A). During the ALI modeling, LPS was administered (0.3 mL) via intratracheal instillation in the ALI and treatment groups, while the control group received an equivalent volume of NS. During the treatment stage, the treatment and ALI groups received daily intraperitoneal injections of DEX (10-mg/kg body weight) or NS, respectively. The first treatment is 1 h post-LPS exposure. One week after intratracheal instillation surgery, all rats underwent sequential ^{129}Xe MRI examinations, PFTs, CT scans, and histology as illustrated in Figure 1A.

To evaluate the potential effects of short-term DEX treatment on lung function in healthy rats, an additional cohort of 10 healthy animals was randomly assigned to two groups: a DEX-treated group and a saline control group. Rats in the DEX group received daily intraperitoneal injections of dexamethasone sodium phosphate (10-mg/kg body weight), while the control group received equivalent volumes of normal saline. Each group received three consecutive injections. One week after the first administration, all animals underwent sequential hyperpolarized ^{129}Xe MR examinations and PFTs.

2.3 | HP ^{129}Xe MR Examinations

All MR examinations were conducted on a 7.0-T animal MRI scanner (Bruker BioSpec 70/20 USR, Germany) equipped with a home-built dual-tuned birdcage coil. Under anesthesia with sodium pentobarbital (40 mg/kg, intraperitoneal), rats were tracheostomized with a 14G endotracheal tube, which was secured with surgical thread to minimize gas leakage. After catheter intubation, rats were placed supine and ventilated alternately with oxygen or HP xenon gas, using a tidal volume of 2.5 mL while maintaining airway pressure below 15-cm H_2O through an MR-compatible gas delivery system. Anesthesia was maintained with 1%–2% isoflurane.

For ventilation imaging, rats were flushed with xenon gases three times to reduce T1 relaxation decay effects. Then, a fast low-angle shot (FLASH) sequence [45] was applied during the breath-hold, utilizing the following parameters: repetition time (TR)/echo time (TE) = 7.6 ms/2.5 ms, flip angle = 10°, centric encoding, number of slices = 7, slice thickness = 4 mm, field of view (FOV) = 50 mm × 50 mm, and matrix = 128 × 128.

For HP ^{129}Xe MR spectroscopy (MRS), a chemical shift saturation recovery (CSSR) sequence was used within a single breath-hold following two xenon flushes [46] (Figure 1B). Two Gaussian-shaped pulses with durations of 0.5 and 0.3 ms were

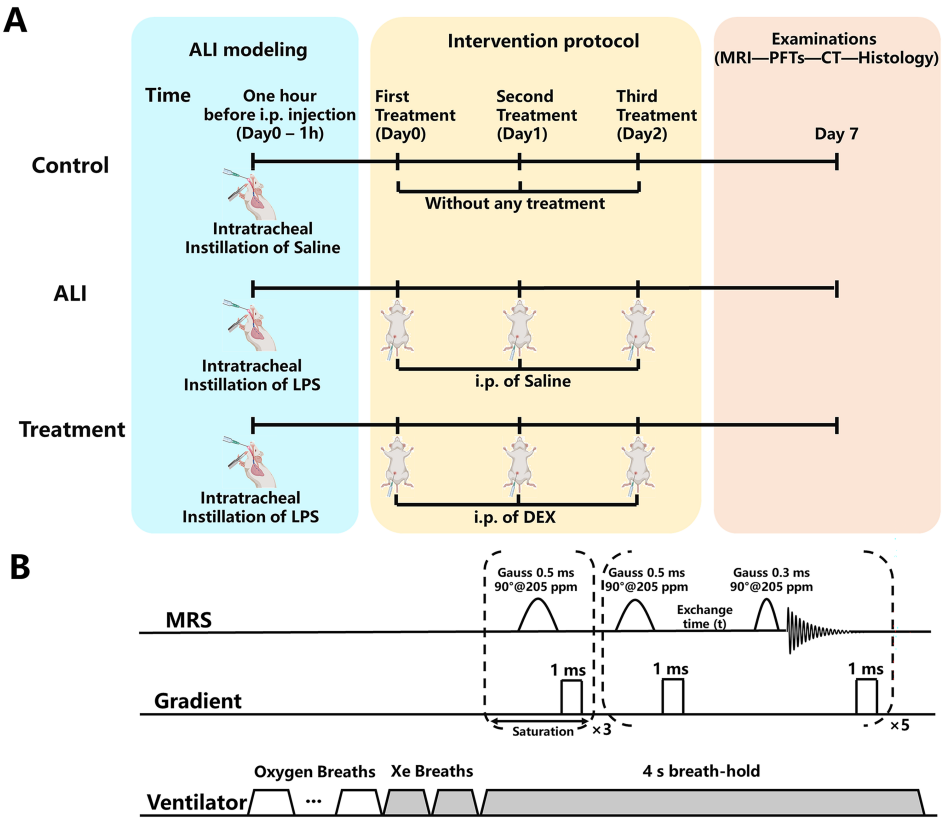

FIGURE 1 | (A) Schematic overview of ALI modeling and intervention protocol, along with the timeline of subsequent examinations. Day 0 marks the start of treatment. (B) Schematic of the breathing strategy and ^{129}Xe MRS pulse sequences for chemical shift saturation recovery (CSSR). Following the final xenon inhalation, ^{129}Xe MR data were collected during a controlled breath-hold. For CSSR data collection, two Gaussian-shaped RF pulses centered at the dissolved ^{129}Xe resonance (approximately 205 ppm) with durations of 0.5 and 0.3 ms were used for saturating and exciting the MR signals of dissolved ^{129}Xe in the lung, respectively. Abbreviations: ALI, acute lung injury; DEX, dexamethasone sodium phosphate; i.p., intraperitoneal injection; LPS, lipopolysaccharide.

used to saturate and excite the dissolved ^{129}Xe signals at approximately 205 ppm, with off-resonance effects corresponding to flip angles of 0.05° and 0.17° on the gas-phase ^{129}Xe, respectively. Spectra were acquired at a 25 kHz bandwidth, with 1024 sampling points, over 24 exchange time points (2–400 ms). Each CSSR sequence was repeated five times per rat.

2.4 | PFTs

PFTs were performed using a commercial Forced Maneuvers system (CRFM 100, EMMS, UK). Following baseline correction, the system inflated the lungs to 30 cmH_2O and briefly maintained this pressure before initiating a forced expiration by connecting the airway to a negative pressure reservoir. Expiration continued until the respiratory flow dropped to zero, with the expiratory rate limited by the animal's pulmonary resistance. FVC was defined as the total volume of air exhaled completely and forcefully after maximal inspiration [47]. The volume exhaled within the first 100 ms following maximal inspiration was defined as the forced expiratory volume in 100 ms (FEV_{100}). Quasi-static compliance (C_{qs}) was calculated from the slope of the pressure–volume curve between 0 and 10 cmH_2O ($\Delta V/\Delta P$). Forced expiratory volume in 100 ms (FEV_{100}), FVC, and quasi-static lung compliance (C_{qs}) were obtained within 5 min.

2.5 | CT Imaging

Following PFTs, rats were imaged in the supine position using a small animal micro-CT (SkyScan 1176, Bruker, Kontich, Belgium). Scans were performed with breath-gating and the following parameters: 80-kVp x-ray voltage, 310-μA current, 1-mm aluminum filter, 100-ms exposure per projection, and 360 projections. The resulting voxel size was $35\times35\times35\,\mu m^3$. Images were reconstructed using NRecon software (SkyScan, NRecon Reconstruction, Kontich, Belgium) and lung parenchyma segmentation [48] was performed in ITK-SNAP (v4.02, http://www.itksnap.org) to calculate mean lung density (MLD).

2.6 | Histology

Following CT imaging, rats were euthanized with an overdose of sodium pentobarbital (150 mg/kg). Lungs were extracted and immersed in 4% paraformaldehyde at 25 cmH_2O for > 2 h, then stored for > 48 h. Tissue samples were embedded in paraffin, sectioned at 5 μm, and stained with hematoxylin and eosin (H&E, Servicebio Technology, Wuhan, China) for histological analysis of inflammation.

2.7 | Data Processing

All the MR data was processed in MATLAB software (The MathWorks Inc., Natick, MA, USA). ^{129}Xe ventilation imaging was reconstructed into images using a two-dimensional Fourier transform. The ^{129}Xe MR FIDs were analyzed using a time-domain fitting approach to quantify the signal amplitudes and chemical shift of ^{129}Xe in the membrane, RBC, and gas phase. This analysis was performed using OXSA toolbox [49], which implements the Advanced Method for Accurate, Robust, and Efficient Spectral (AMARES) fitting approach. Ratios of Mem/Gas, RBC/Mem and ^{129}Xe chemical shift in RBC were derived from the ^{129}Xe spectrum with an exchange time of 100 ms. Gas-exchange parameters, including septal wall thickness (d), surface area to volume ratio (SVR), barrier-to-septum ratio (δ/d), the air-capillary barrier thickness (δ), hematocrit (Hct), and pulmonary capillary transit time (t_x) were extracted by fitting the CSSR data to the model of xenon exchange (MOXE) [50, 51].

2.8 | Statistical Analysis

All the statistical analyses were performed using SPSS 29.0 (IBM Corp., Armonk, NY, USA), except for the Conover–Iman post hoc tests, which were conducted using R software (version 4.5.1). Data were presented as medians and interquartile range (IQR). Inter-group comparisons of ^{129}Xe MRS, PFTs and CT results were assessed using Kruskal–Wallis tests followed by Conover–Iman multiple comparison tests. Correlations between ^{129}Xe MRS-derived parameters and other measurements were evaluated using Pearson correlation analysis. A p value < 0.05 was considered statistically significant.

3 | Results

3.1 | HP ^{129}Xe MR and CT Scans

Figure 2 presents typical ^{129}Xe ventilation images, CT images, and CSSR uptake curves for each group, respectively. In ^{129}Xe images, both ALI and DEX-treated rats exhibited distinct poorly ventilated areas in the right upper lobes compared to the control rat. Notably, the DEX intervention group showed a mild improvement in pulmonary aeration condition relative to the untreated ALI rat. This finding is further supported by the CT images, where high-density parenchymal opacifications were observed in the LPS-induced ALI rat. In contrast, these opacifications were attenuated in the DEX-administered rat. Quantitative results from the CT scans indicated a statistically significant elevation in MLD in the ALI group compared to both the control group (median, −843.55 HU [IQR: 46.78 HU] vs. −874.51 HU [IQR: 9.26 HU], $p = 0.019$) and the treatment group (median, −843.55 HU [IQR: 46.78 HU] vs. 878.19 HU [IQR: 23.91 HU], $p = 0.011$), as summarized in Table 1. Additionally, in the CSSR uptake curves, the normalized Mem signal curve was markedly elevated in the ALI rat, while only a slight increase was observed in the DEX-treated rat compared to the healthy control rat.

Group-wise comparisons of HP ^{129}Xe MRS-derived physiological parameters are illustrated in Figure 3, with quantitative indices are summarized in Table 1. The median Mem/Gas ratio was significantly higher in the ALI group (0.033 [IQR, 0.005]) relative to that in both control group (0.024 [IQR, 0.003], $p < 0.01$) and DEX group (0.025 [IQR, 0.005], $p < 0.05$). Additionally, RBC/Mem ratio in the ALI group (median, 0.356 [IQR, 0.035]) was substantially reduced compared to those in both the control group (median, 0.607 [IQR, 0.086], $p < 0.001$) and the treatment group (median, 0.431 [IQR, 0.082], $p < 0.001$), whereas a

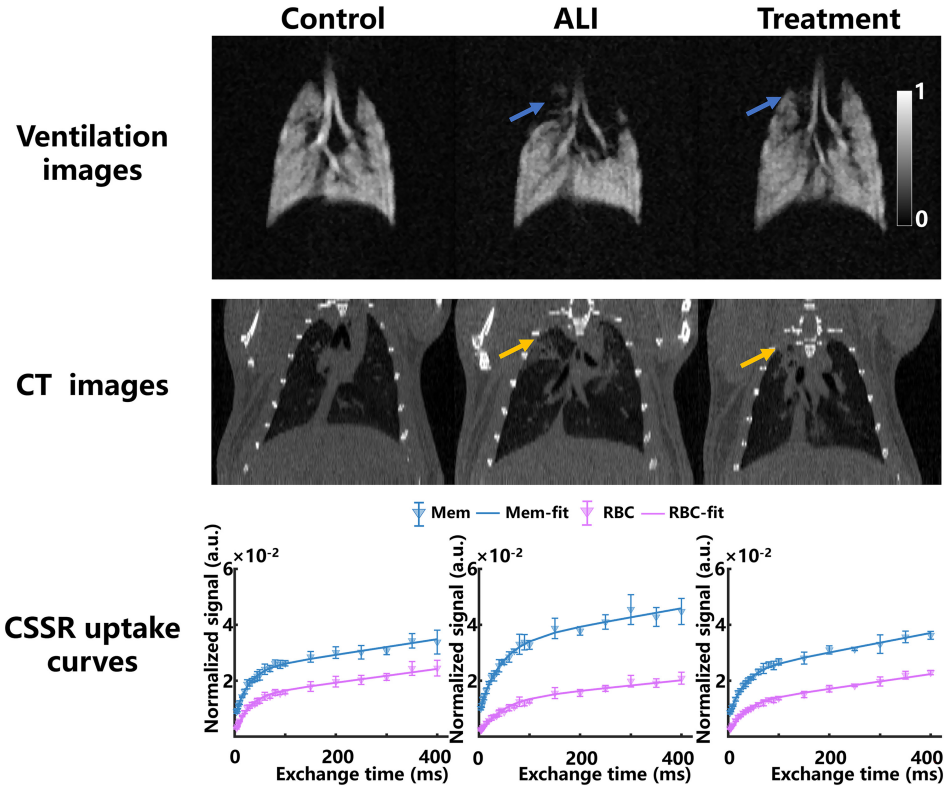

FIGURE 2 | Representative ventilation images, CT images and CSSR uptake curves from the control group (left column), ALI group (middle column), and treatment group (right column). Blue and yellow arrows indicate low ventilation and high-density area in ^{129}Xe MR and CT images, respectively. The dissolved-phase ^{129}Xe signals in the membrane tissue (Mem) and red blood cells (RBCs) were normalized to the gas-phase xenon signal. Abbreviations: ALI, acute lung injury; CSSR, chemical shift saturation recovery; CT, computed tomography.

significant difference was also observed between the treatment and control groups ($p < 0.001$, Figure 3A).

Air-capillary barrier thickness (δ) increased in both ALI and treatment groups compared to the control group ($p < 0.001$ and $p = 0.005$, respectively), whereas the treatment group revealed a mild, though not statistically significant decline compared to the ALI group (Figure 3B). The median δ was 0.870 μm (IQR, 0.151 μm) in the control group, 1.384 μm (IQR, 0.241 μm) in the ALI group, and 1.115 μm (IQR, 0.228 μm) in the treatment group. Additionally, significant intergroup differences in Hct were also observed (Figure 3C). Besides the gas exchange parameters above, we also observed that the chemical shift of RBC (ω_{RBC}) in the ALI group was significantly lower than that in the control group (median 210.406 ppm [IQR, 0.161 ppm] vs. 210.824 ppm [IQR, 0.196 ppm], $p < 0.01$, Figure 3D).

3.2 | PFTs Analysis

Compared to the control group, the ALI group exhibited a significant reduction in FVC (ALI: median 8.0 mL [IQR, 1.5 mL] vs. Control: median 10.9 mL [IQR, 3.1 mL], $p = 0.002$). Moreover, the median FVC in the treatment group was 11.2 mL (IQR, 2.6 mL), which was comparable to that in the control group ($p = 1.000$) and significantly higher than that in the ALI group ($p = 0.004$). No significant differences were observed among the groups for FEV_{100} and C_{qs}. All the quantitative results are summarized in Table 1.

3.3 | Histological Observations

Figure 4 shows representative histological sections from the three groups. The control group exhibited normal alveolar architecture with intact septa and clear airspaces. In contrast, intratracheal administration of LPS induced pronounced inflammatory cell infiltration within the alveolar septa, accompanied by partial alveolar collapse. The ALI group also showed interstitial edema and widening of the alveolar septa, indicating substantial structural damage. However, these pathological alterations were markedly alleviated in the treatment rats, demonstrating reduced inflammatory infiltration and partial restoration of normal lung architecture.

3.4 | Correlations Among ^{129}Xe MRS, PFTs, and CT Parameters

Correlation analysis among RBC/Mem, Hct, δ, and FVC or MLD measurements across the control, ALI, and treatment groups are presented in Figure 5. Positive correlations were observed between FVC and both RBC/Mem ratio ($r = 0.625$, $p < 0.05$, Figure 5A) and Hct ($r = 0.609$, $p < 0.05$, Figure 5B). In contrast, δ showed a negative correlation with FVC ($r = -0.637$, $p < 0.05$, Figure 5C). Additionally, both the RBC/Mem ratio and Hct were negatively correlated with MLD measurements ($r = -0.627$, $p < 0.05$, Figure 5D and $r = -0.695$, $p < 0.01$, Figure 5E, respectively), while δ was positively correlated with MLD ($r = 0.598$, $p < 0.05$, Figure 5F).

TABLE 1 | Summary of statistical results for PFTs, CT, and HP ^{129}Xe MR across all the subjects.

Parameters	Control ($n=5$)	ALI ($n=5$)	Treatment ($n=5$)	p		
				Control–ALI	ALI–treatment	Control–treatment
PFTs						
FEV_{100} (mL)	4.1 (3.0–5.0)	4.4 (3.5–5.4)	4.3 (3.6–4.5)	1.000	1.000	1.000
FVC (mL)	10.9 (9.9–13.0)	8.0 (7.0–8.5)	11.2 (9.2–11.8)	**0.002**	**0.004**	1.000
C_{qs} (mL/cmH_2O)	0.7 (0.6–0.8)	0.5 (0.4–0.7)	0.7 (0.6–0.8)	0.350	0.200	1.000
CT						
MLD (HU)	−874.51 (−879.75 to −870.49)	−843.55 (−859.35 to −812.57)	−878.19 (−885.75 to −861.84)	**0.019**	**0.011**	1.000
Gas-transfer function						
RBC/Mem	0.607 (0.576–0.662)	0.356 (0.345–0.380)	0.431 (0.409–0.491)	**<0.001**	**<0.001**	**<0.001**
Mem/Gas	0.024 (0.021–0.024)	0.033 (0.028–0.033)	0.025 (0.022–0.027)	**0.004**	**0.031**	0.814
d (um)	9.612 (8.783–9.897)	11.414 (10.014–13.585)	10.841 (10.018–12.928)	0.082	1.000	0.129
SVR	362.3 (332.1–377.0)	371.3 (362.9–410.8)	347.5 (281.1–348.2)	0.402	**0.022**	0.402
δ/d	0.087 (0.079–0.105)	0.121 (0.101–0.138)	0.105 (0.092–0.122)	0.160	0.900	0.900
t_x (ms)	564.0 (282.2–625.8)	644.6 (423.5–700.6)	467.4 (389.3–685.7)	1.000	1.000	1.000
δ (um)	0.870 (0.774–0.925)	1.384 (1.265–1.506)	1.115 (1.098–1.326)	**<0.001**	0.113	**0.005**
Hct	0.296 (0.283–0.314)	0.216 (0.206–0.225)	0.242 (0.235–0.266)	**<0.001**	**<0.001**	**<0.001**
ω_{RBC} (ppm)	210.824 (210.666–210.862)	210.406 (210.368–210.529)	210.684 (210.526–210.789)	**0.006**	0.058	0.762

Note: Data were presented as medians and interquartile range (25th–75th percentile) for each group. Intergroup comparison of quantitative parameters was analyzed using the Kruskal–Wallis test. The p values were calculated among the three groups with significant differences in bold, and significance was set at $p<0.05$.
Abbreviations: δ, the air-capillary barrier thickness; δ/d, the ratio of barrier thickness to interstitial thickness; ω_{RBC}, ^{129}Xe chemical shift in red blood cells; ALI, acute lung injury; C_{qs}, quasi-static lung compliance; CT, computed tomography; d, the alveolar septal thickness; FEV_{100}, forced expiratory volume in 100 ms; FVC, forced vital capacity; Hct, hematocrit; Mem/Gas, the ratio of ^{129}Xe signal in membrane tissue to that in alveolus; MLD, mean lung density; PFTs, pulmonary function tests; RBC/Mem, the ratio of ^{129}Xe signal in red blood cells to that in membrane tissue; SVR, the alveolar surface area-to-volume ratio; t_x, the capillary transit time.

4 | Discussion

The goal of this study is to demonstrate the feasibility of HP ^{129}Xe MR for detecting therapeutic effects of dexamethasone sodium phosphate (DEX) in an LPS-induced ALI rat model. Our results indicate that ^{129}Xe MR-derived parameters—including RBC/Mem, Mem/Gas, Hct—are sensitive to the therapeutic effects of DEX on lung injury. ^{129}Xe MRI revealed that there was a significant elevation in pulmonary function in the DEX treatment group, though not fully returned to normal levels. Such a sensitive assessment of lung function is not currently possible by PFTs. Although the therapeutic effects of glucocorticoid in LPS-induced lung injury are well documented, this represents the first in vivo application of HP ^{129}Xe MR for assessment of glucocorticoid efficacy in ALI.

One week following LPS instillation, the ALI group exhibited an approximately 41% reduction in RBC/Mem ratio compared with the control group, corroborating previous findings [38, 52]. Following DEX treatment, normalization of the RBC/Mem ratio may be attributed to two primary factors. First, the pathology of the treatment group indicated a reduction in interstitial edema, which alleviated capillary compression and decreased vascular resistance. These enhance local blood flow perfusion and facilitate the transport of xenon from the lung interstitial to RBCs [33], resulting in an increased RBC/Mem ratio. Additionally, dexamethasone has been shown to inhibit neutrophil infiltration in the alveoli and reduce levels of pro-inflammatory cytokines and oxidative stress markers [53, 54]. These actions may contribute to a mild decrease in the thickness of the gas exchange membrane, thereby reducing the amount of dissolved ^{129}Xe within it and leading to a lower Mem/Gas ratio. These findings are consistent with previous studies demonstrating that dexamethasone reduces protein concentration and neutrophil counts in bronchoalveolar lavage fluids [55]. The RBC/Mem ratio in DEX-treated rats remained significantly lower than that of the control group, indicating only partial restoration of gas exchange function. Notably, this residual dysfunction was not detected by conventional PFTs or CT, highlighting the superior sensitivity of HP ^{129}Xe MR-derived biomarkers for detecting subtle pulmonary abnormalities. It should be noted that diffusion capacity of the lung for carbon monoxide (DL_{CO}) measurement was not performed due to the absence of a gas chromatograph

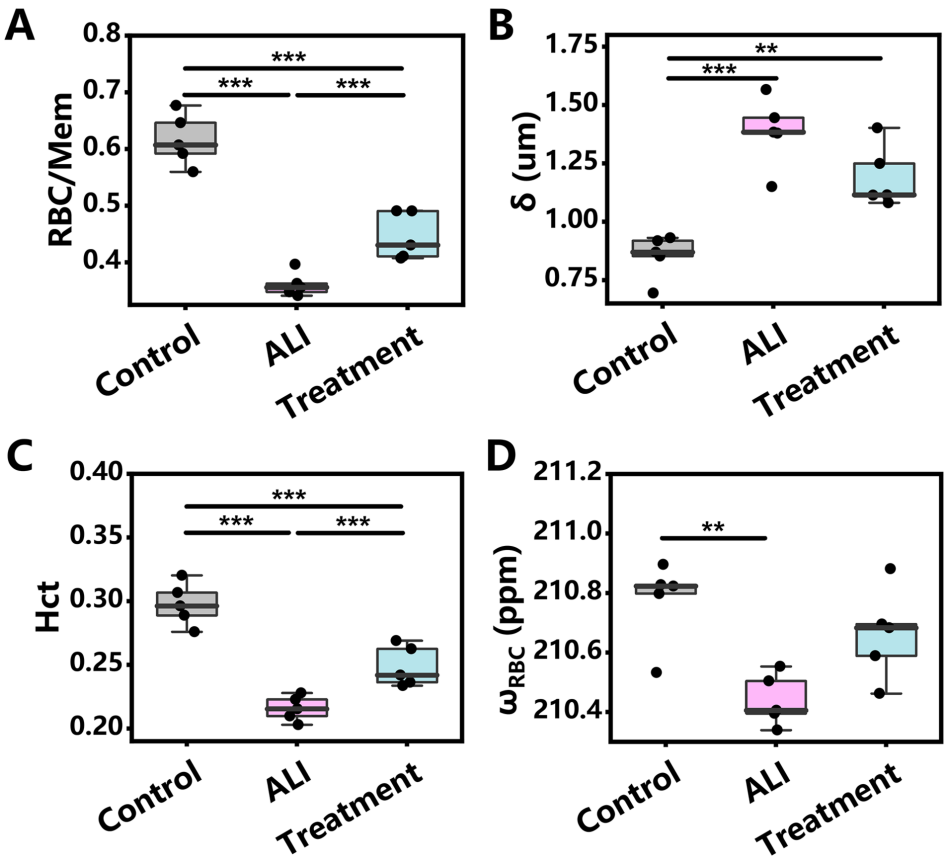

FIGURE 3 | Comparison of measured physiological parameters among the three groups using hyperpolarized ^{129}Xe MR. (A) RBC/Mem; (B) the air-capillary barrier thickness (δ); (C) hematocrit (Hct); (D) ^{129}Xe chemical shift in red blood cells (ω_{RBC}). Each black dot is an individual study subject. The long horizontal solid lines are first quartile, median, and third quartile, respectively. Asterisks denote significant differences between two cohorts, as determined by Kruskal–Wallis test following by post hoc Conover–Iman test. $^{**}p < 0.01$, $^{***}p < 0.001$. Abbreviations: ALI, acute lung injury; RBC/Mem, the ratio of ^{129}Xe signal in red blood cells to that in membrane tissue.

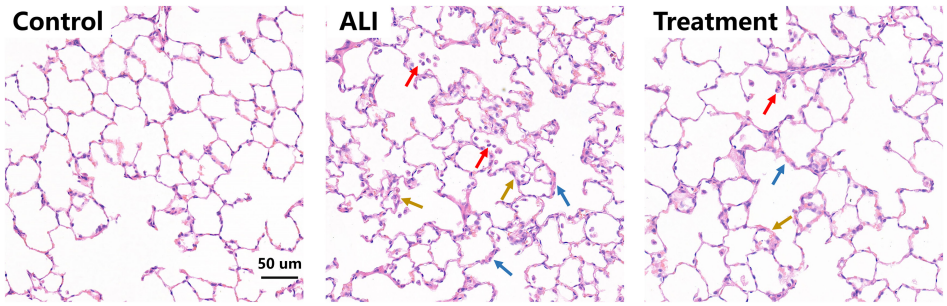

FIGURE 4 | Representative H&E-stained lung sections from the control, ALI, and treatment groups. Inflammatory cell infiltration is evident within the alveolar spaces (red arrows), accompanied by interstitial edema (blue arrows) and partial destruction of alveolar architecture (golden arrows) in the ALI group. The treatment group shows partial structural recovery with reduced inflammatory infiltration. Abbreviations: ALI, acute lung injury.

for small-animal assessments, representing a methodological limitation of this study.

Hct reduction in rats receiving LPS treated with normal saline was consistent with previous LPS-induced lung injury models [38]. DEX treatment increased Hct by approximately 12% in the treatment group, indicative of improved oxygen-carrying capacity. However, this elevation is more likely due to DEX-mediated improvements in ventilation and perfusion, possibly through blood flow redistribution to newly ventilated areas [56]. First, the anti-inflammatory effects of DEX improve airway obstruction and lung edema, as evidenced by ventilation images showing an obvious reduction in the area of hypoventilation regions. This leads to a decrease in localized abnormal blood flow distribution [57] and an increase in perfusion in normally ventilated areas. Second, endothelial permeability reduction [58] resulted in an overall increase in pulmonary blood flow and circulating blood volume. These findings are consistent with previous studies confirming that glucocorticoids can significantly optimize pulmonary ventilation function in patients with asthma

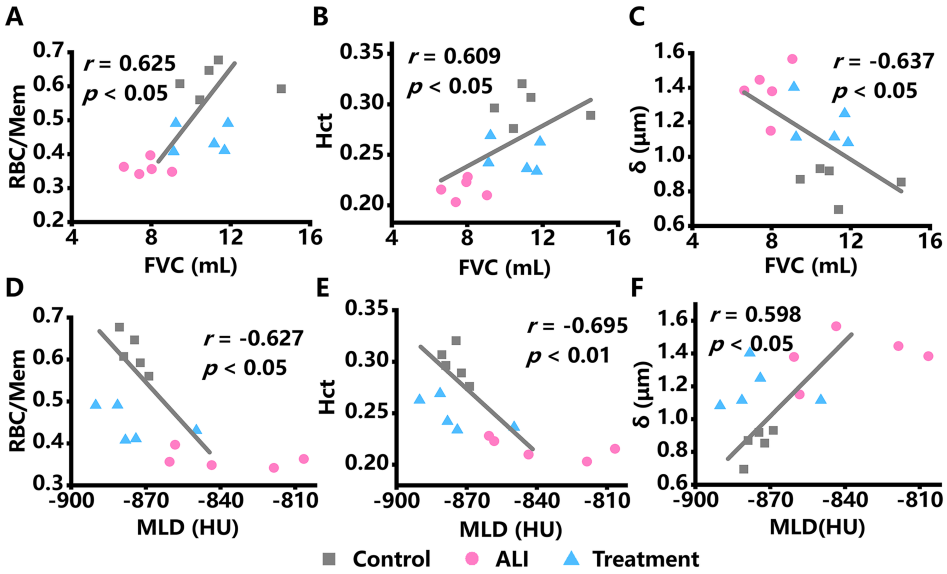

FIGURE 5 | Correlations between HP ^{129}Xe MRS-derived parameters (RBC/Mem, Hct, δ), PFTs-derived parameters (forced vital capacity, FVC), and CT-derived parameters (mean lung density, MLD) in the control, ALI, and treatment groups (A–F). Pearson correlation coefficients (r) and corresponding p values are indicated in each panel. Significant correlations were found between the FVC or MLD, and the measured the ratio of ^{129}Xe signal in red blood cells to that in membrane tissue (RBC/Mem), hematocrit (Hct), and the air-capillary barrier thickness (δ). Abbreviations: ALI, acute lung injury.

[59] and endotoxin-induced pulmonary inflammation model [60]. Furthermore, the observed correlation between Hct and MLD or FVC supports the notion Hct normalization is driven by the anti-inflammatory effects of DEX [61]. Additionally, control experiments conducted in healthy rats only injected with DEX (DEX group) or normal saline (control group) showed no significant differences in lung function parameters (Table S1, $p > 0.05$ for all parameters), suggesting that the short-term DEX treatment protocol had little effect on lung function of healthy rats.

Besides gas exchange parameters, the chemical shift of xenon in RBCs (ω_{RBC}) showed a significant reduction in the ALI group compared to that in the control group. Our findings are consistent with the results of in vitro and human studies by Norquay et al. [62] and with Friedlander's work in rats [63], both of which demonstrated that anoxia shifts the RBC resonance peak toward a lower frequency.

As a proof-of-concept study, our research can be extended in following ways: First, the RBC/Mem ratio in the treatment group has not yet normalized, indicating the potential presence of residual underlying pathology. The residual pathology observed in the present study is unlikely to be attributable solely to the 7-day treatment protocol. Previous work has demonstrated that similar therapeutic regimens do not achieve complete resolution of lung pathology in ALI models, even at later time points such as Day 14 or Day 28 [58, 64]. Consistent with these findings, extended dexamethasone treatment has been reported to be insufficient to fully restore lung structure and function to baseline levels [65, 66]. This limited response may reflect saturation of glucocorticoid receptors [67], beyond which additional treatment provides diminishing therapeutic benefit. Furthermore, ALI is frequently accompanied by fibrotic remodeling [38]. Although dexamethasone has been shown to attenuate fibrotic progression, it does not reverse established fibrosis, which may contribute to persistent impairment of pulmonary gas exchange [68]. Future studies evaluating optimized dosing strategies and combination therapies may help to further improve functional recovery in ALI. Second, to enhance the translational relevance of the findings, it is necessary to incorporate widely used clinical assessments—such as monitoring respiratory metric and arterial blood gas analysis—in addition to CT and PFTs, providing a more comprehensive framework for personalized care. Furthermore, conducting longitudinal imaging of these animals would have been preferable, as it would allow each subject to serve as its own control and more closely simulate clinical realities. In addition, transitioning from whole-lung metrics (e.g., CSSR) to spatially resolved methods—such as Dixon-based 3D imaging of the airspace, membrane, and RBC compartments—or alternatively employing the xenon transfer contrast (XTC) technique [69]—could enhance the assessment of regional lung function and spatial heterogeneity. The clinical significance of this approach is underscored by recent evidence identifying elevated membrane uptake as a treatable trait in several forms of interstitial lung diseases. Despite the broader physiological insights provided by CSSR, the global RBC/Mem ratio remains the most reliable and reproducible parameter across studies. Additionally, ^{129}Xe MRI examinations present significant challenges for patients with ALI, primarily due to the incompatibility between essential life-support equipment and the controlled environment of the MRI suite. However, ^{129}Xe MRI may still hold promise for longitudinal evaluation of treatment response and pulmonary recovery in convalescent patients following ICU discharge. Moreover, this technique remains a powerful tool for preclinical studies, enabling detailed investigation of disease progression and therapeutic interventions in experimental models of ALI.

5 | Conclusion

This study demonstrates the feasibility of HP ^{129}Xe MR in quantifying therapeutic effects of dexamethasone (DEX) in ALI rat

models. Our findings show that ^{129}Xe MR-derived parameters are sensitive to the therapeutic response of ALI compared to conventional PFTs and CT metrics. These results highlight the potential of HP ^{129}Xe MR as a non-invasive tool for monitoring therapeutic efficacy in ALI.

Author Contributions

X.Z., Y.Z., and Haidong Li conceived this study and designed the experimental protocols. MRI scanning was performed by Y.Z., M.Z., X.L., and Hongchuang Li. Data acquisition was conducted by Y.Z., M.Y., W.W., J.Z., X.Z., H.L., S. W, and Y.H. Data analysis was conducted by Y.Z., M.Z., X.L., and Hongchuang Li. Interpretation of the data was carried out by X.Z., Y.Z., Haidong Li, and M.Z. The manuscript was drafted by X.Z., Y.Z., Haidong Li, and M.Z. All authors have read and approved the final version of the manuscript.

Acknowledgments

This work was supported by National Natural Science Foundation of China (82441015, T2522037, and 82272109), the Strategic Priority Research Program of the Chinese Academy of Sciences (XDC0170000 and XDB0540000), Scientific Instrument Developing Project of the Chinese Academy of Sciences (PTYQ2024TD0001), Key Research Program of Frontier Sciences, CAS (ZDBS-LY-JSC004), and Hubei Province Science and Technology Innovation Talent Program (2024DJA001).

Funding

This work was supported by National Natural Science Foundation of China (82441015, T2522037, and 82272109), Strategic Priority Research Program of the Chinese Academy of Sciences (XDC0170000 and XDB0540000), Key Research Program of Frontier Science, Chinese Academy of Sciences (ZDBS-LY-JSC004), Scientific Instrument Developing Project of the Chinese Academy of Sciences (PTYQ2024TD0001), and Hubei Province Science and Technology Innovation Talent Program (2024DJA001).

Conflicts of Interest

The authors declare no conflicts of interest.

Data Availability Statement

The data that support the findings of this study are available from the corresponding author upon reasonable request.

References

1. J. Zhang, Y. Guo, M. Mak, and Z. Tao, "Translational Medicine for Acute Lung Injury," *Journal of Translational Medicine* 22, no. 1 (2024): 25.

2. P. Z. Mannes, C. E. Barnes, J. Biermann, et al., "Molecular Imaging of Chemokine-Like Receptor 1 (CMKLR1) in Experimental Acute Lung Injury," *Proceedings of the National Academy of Sciences of The United States of America* 120, no. 3 (2023): e2216458120.

3. Q. Yuan, A. Basit, W. Liang, et al., "Pazopanib Ameliorates Acute Lung Injuries via Inhibition of MAP 3K2 and MAP 3K3," *Science Translational Medicine* 13, no. 591 (2021): eabc2499.

4. T. Kido, K. Muramatsu, K. Yatera, et al., "Efficacy of Early Sivelestat Administration on Acute Lung Injury and Acute Respiratory Distress Syndrome," *Respirology* 22, no. 4 (2017): 708–713.

5. T. Rhen and J. A. Cidlowski, "Antiinflammatory Action of Glucocorticoids—New Mechanisms for Old Drugs," *New England Journal of Medicine* 353, no. 16 (2005): 1711–1723.

6. S. Yoshihiro, T. Hongo, S. Ohki, et al., "Steroid Treatment in Patients With Acute Respiratory Distress Syndrome: A Systematic Review and Network Meta-Analysis," *Journal of Anesthesia* 36, no. 1 (2022): 107–121.

7. F. Chen, L. Hao, S. Zhu, et al., "Potential Adverse Effects of Dexamethasone Therapy on COVID-19 Patients: Review and Recommendations," *Infectious Diseases and Therapy* 10, no. 4 (2021): 1907–1931.

8. P. Mikolka, P. Kosutova, M. Kolomaznik, et al., "Effect of Different Dosages of Dexamethasone Therapy on Lung Function and Inflammation in an Early Phase of Acute Respiratory Distress Syndrome Model," *Physiological Research* 68 (2019): S253–S263.

9. V. M. Ranieri, G. D. Rubenfeld, B. T. Thompson, et al., "Acute Respiratory Distress Syndrome: The Berlin Definition," *Journal of the American Medical Association* 307, no. 23 (2012): 2526–2533.

10. Y. Xin, M. Cereda, N. Yehya, et al., "Imatinib Alleviates Lung Injury and Prolongs Survival in Ventilated Rats," *American Journal of Physiology. Lung Cellular and Molecular Physiology* 322, no. 6 (2022): L866–L872.

11. B. Bouhemad, H. Brisson, M. Le-Guen, C. Arbelot, Q. Lu, and J. J. Rouby, "Bedside Ultrasound Assessment of Positive End-Expiratory Pressure-Induced Lung Recruitment," *American Journal of Respiratory and Critical Care Medicine* 183, no. 3 (2011): 341–347.

12. M. R. Smit, P. H. Mayo, and S. Mongodi, "Lung Ultrasound for Diagnosis and Management of ARDS," *Intensive Care Medicine* 50, no. 7 (2024): 1143–1145.

13. S. Mongodi, D. De Luca, A. Colombo, et al., "Quantitative Lung Ultrasound: Technical Aspects and Clinical Applications," *Anesthesiology* 134, no. 6 (2021): 949–965.

14. M. Cereda, Y. Xin, A. Goffi, et al., "Imaging the Injured Lung: Mechanisms of Action and Clinical Use," *Anesthesiology* 131, no. 3 (2019): 716–749.

15. A. Pesenti, G. Musch, D. Lichtenstein, et al., "Imaging in Acute Respiratory Distress Syndrome," *Intensive Care Medicine* 42, no. 5 (2016): 686–698.

16. H. E. Möller, X. J. Chen, B. Saam, et al., "MRI of the Lungs Using Hyperpolarized Noble Gases," *Magnetic Resonance in Medicine* 47, no. 6 (2002): 1029–1051.

17. K. Ruppert, J. F. Mata, J. R. Brookeman, K. D. Hagspiel, and J. P. Mugler, 3rd, "Exploring Lung Function With Hyperpolarized ^{129}Xe Nuclear Magnetic Resonance," *Magnetic Resonance in Medicine* 51, no. 4 (2004): 676–687.

18. I. Dregely, J. P. Mugler, 3rd, I. C. Ruset, et al., "Hyperpolarized Xenon-129 Gas-Exchange Imaging of Lung Microstructure: First Case Studies in Subjects With Obstructive Lung Disease," *Journal of Magnetic Resonance Imaging* 33, no. 5 (2011): 1052–1062.

19. Y. Yang, S. Yue, L. Shen, et al., "Ultrasensitive ^{129}Xe Magnetic Resonance Imaging: From Clinical Monitoring to Molecular Sensing," *Advancement of Science* 12, no. 8 (2025): e2413426.

20. A. L. Kern, D.-H. Park, J. Fuge, et al., "Loss of Pulmonary Capillaries in Idiopathic Pulmonary Arterial Hypertension With Low Diffusion Capacity Is Accompanied by Early Diffuse Emphysema Detected by ^{129}Xe MRI," *European Radiology* 35, no. 6 (2024): 3010–3020.

21. A. Ouriadov, F. Guo, D. G. McCormack, and G. Parraga, "Accelerated ^{129}Xe MRI Morphometry of Terminal Airspace Enlargement: Feasibility in Volunteers and Those With Alpha-1 Antitrypsin Deficiency," *Magnetic Resonance in Medicine* 84, no. 1 (2020): 416–426.

22. M. Zhang, H. Li, H. Li, et al., "Assessment of Lung Microvasculature Alterations in Pulmonary Fibrosis With Hyperpolarized Xenon Magnetic Resonance," *Magnetic Resonance in Medicine* (2026), https://doi.org/10.1002/mrm.70279.

23. H. Li, Z. Zhang, X. Zhao, et al., "Quantitative Evaluation of Pulmonary Gas-Exchange Function Using Hyperpolarized ^{129}Xe CEST MRS and MRI," *NMR in Biomedicine* 31, no. 9 (2018): e3961.

24. A. M. Matheson, A. S. Bdaiwi, M. M. Willmering, et al., "Disease Classification of Pulmonary Xenon Ventilation MRI Using Artificial Intelligence," *Academic Radiology* 32 (2025): 6330–6342, https://doi.org/10.1016/j.acra.2025.06.024.

25. D. Singh, J. M. Wild, D. Saralaya, et al., "Effect of Indacaterol/Glycopyrronium on Ventilation and Perfusion in COPD: A Randomized Trial," *Respiratory Research* 23, no. 1 (2022): 26.

26. Q. Rao, H. Li, Q. Zhou, et al., "Assessment of Pulmonary Physiological Changes Caused by Aging, Cigarette Smoking, and COPD With Hyperpolarized ^{129}Xe Magnetic Resonance," *European Radiology* 34, no. 11 (2024): 7450–7459.

27. H. Li, H. Li, M. Zhang, et al., "Advancements and Applications of Hyperpolarized Xenon MRI for COPD Assessment in China," *British Journal of Radiology* (2025): tqaf119, https://doi.org/10.1093/bjr/tqaf119.

28. S. S. Kaushik, Z. I. Cleveland, G. P. Cofer, et al., "Diffusion-Weighted Hyperpolarized ^{129}Xe MRI in Healthy Volunteers and Subjects With Chronic Obstructive Pulmonary Disease," *Magnetic Resonance in Medicine* 65, no. 4 (2011): 1154–1165.

29. E. Kieninger, S. Munidasa, M. Curdy, et al., "Application of the Defect Distribution Index to Functional Lung MRI of Pediatric Cystic Fibrosis Lung Disease and Controls," *Journal of Cystic Fibrosis* 24 (2025): 809–815, https://doi.org/10.1016/j.jcf.2025.02.015.

30. A. S. Bdaiwi, D. J. Roach, M. E. West, et al., "Longitudinal Monitoring of Lumacaftor/Ivacaftor Response in Young Children With Cystic Fibrosis Lung Disease Using ^{129}Xe MRI," *Academic Radiology* 32 (2025): 6238–6249, https://doi.org/10.1016/j.acra.2025.06.042.

31. L. L. Walkup, R. P. Thomen, T. G. Akinyi, et al., "Feasibility, Tolerability and Safety of Pediatric Hyperpolarized ^{129}Xe Magnetic Resonance Imaging in Healthy Volunteers and Children With Cystic Fibrosis," *Pediatric Radiology* 46, no. 12 (2016): 1651–1662.

32. E. Durom, C. Yang, A. Mozaffaripour, et al., "Quantification of ^{129}Xe MRI Ventilation-Defect-Percent Using Binary-Threshold, Gaussian Linear-Binning and K-Means Methods: Differences in Asthma and COPD," *Academic Radiology* 32, no. 8 (2025): 4893–4902.

33. A. Costelle, J. Lu, S. Leewiwatwong, et al., "Combining Hyperpolarized ^{129}Xe MR Imaging and Spectroscopy to Noninvasively Estimate Pulmonary Vascular Resistance," *Journal of Applied Physiology* 138, no. 3 (2025): 623–633.

34. R. S. Virgincar, J. C. Nouls, Z. Wang, et al., "Quantitative ^{129}Xe MRI Detects Early Impairment of Gas-Exchange in a Rat Model of Pulmonary Hypertension," *Scientific Reports* 10, no. 1 (2020): 7385.

35. D. G. Mummy, E. M. Coleman, Z. Wang, et al., "Regional Gas Exchange Measured by ^{129}Xe Magnetic Resonance Imaging Before and After Combination Bronchodilators Treatment in Chronic Obstructive Pulmonary Disease," *Journal of Magnetic Resonance Imaging* 54, no. 3 (2021): 964–974.

36. A. D. Hahn, K. J. Carey, G. P. Barton, et al., "Functional Xenon-129 Magnetic Resonance Imaging Response to Antifibrotic Treatment in Idiopathic Pulmonary Fibrosis," *ERJ Open Research* 9, no. 3 (2023): 00080–02023.

37. F. Alenezi, A. Costelle, P. Sharma, et al., "Xenon-129 Magnetic Resonance Imaging and Spectroscopy Detects Response to Therapy in Pulmonary Hypertension," *European Respiratory Journal* 65, no. 2 (2025): 2401651.

38. M. Zhang, H. Li, H. Li, et al., "Dynamic Evaluation of Acute Lung Injury Using Hyperpolarized ^{129}Xe Magnetic Resonance," *NMR in Biomedicine* 37, no. 4 (2024): e5078.

39. S. Månsson, J. Wolber, B. Driehuys, P. Wollmer, and K. Golman, "Characterization of Diffusing Capacity and Perfusion of the Rat Lung in a Lipopolysaccaride Disease Model Using Hyperpolarized ^{129}Xe," *Magnetic Resonance in Medicine* 50, no. 6 (2003): 1170–1179.

40. H. Li, H. Li, M. Zhang, C. Huang, and X. Zhou, "Direct Imaging of Pulmonary Gas Exchange With Hyperpolarized Xenon MRI," *Innovation* 5, no. 6 (2024): 100720.

41. H. S. Kulkarni, J. S. Lee, J. A. Bastarache, et al., "Update on the Features and Measurements of Experimental Acute Lung Injury in Animals: An Official American Thoracic Society Workshop Report," *American Journal of Respiratory Cell and Molecular Biology* 66, no. 2 (2022): e1–e14.

42. V. Neiens, E. M. Hansbauer, T. J. Jaquin, et al., "Preclinical Concept Studies Showing Advantage of an Inhaled Anti-CTGF/CCN2 Protein for Pulmonary Fibrosis Treatment," *Nature Communications* 16, no. 1 (2025): 3251.

43. J. Nouls, M. Fanarjian, L. Hedlund, and B. Driehuys, "A Constant-Volume Ventilator and Gas Recapture System for Hyperpolarized Gas MRI of Mouse and Rat Lungs," *Concepts in Magnetic Resonance, Part B, Magnetic Resonance Engineering* 39b, no. 2 (2011): 78–88.

44. H. L. Du, A. D. Zhai, and H. Yu, "Synergistic Effect of Halofuginone and Dexamethasone on LPS-Induced Acute Lung Injury in Type II Alveolar Epithelial Cells and a Rat Model," *Molecular Medicine Reports* 21, no. 2 (2020): 927–935.

45. M. Zhang, H. Li, Y. Xiao, et al., "Assessment of Global and Regional Lung Compliance in Pulmonary Fibrosis With Hyperpolarized Gas MRI," *Journal of Magnetic Resonance Imaging* 61, no. 3 (2025): 1404–1415.

46. M. Zhang, H. Li, H. Li, et al., "Quantitative Evaluation of Lung Injury Caused by $PM_{2.5}$ Using Hyperpolarized Gas Magnetic Resonance," *Magnetic Resonance in Medicine* 84, no. 2 (2020): 569–578.

47. E. Bonnardel, R. Prevel, M. Campagnac, et al., "Determination of Reliable Lung Function Parameters in Intubated Mice," *Respiratory Research* 20, no. 1 (2019): 211–224.

48. R. Baron, S. Kadlecek, L. Loza, et al., "Deriving Regionally Specific Biomarkers of Emphysema and Small Airways Disease Using Variable Threshold Parametric Response Mapping on Volumetric Lung CT Images," *Academic Radiology* 29, no. Suppl 2(Suppl 2) (2022): S127–s136.

49. L. A. B. Purvis, W. T. Clarke, L. Biasiolli, L. Valkovič, M. D. Robson, and C. T. Rodgers, "OXSA: An Open-Source Magnetic Resonance Spectroscopy Analysis Toolbox in MATLAB," *PLoS ONE* 12, no. 9 (2017): e0185356.

50. Y. V. Chang, "MOXE: A Model of Gas Exchange for Hyperpolarized ^{129}Xe Magnetic Resonance of the Lung," *Magnetic Resonance in Medicine* 69, no. 3 (2013): 884–890.

51. H. Li, X. Zhao, Y. Wang, et al., "Damaged Lung Gas Exchange Function of Discharged COVID-19 Patients Detected by Hyperpolarized ^{129}Xe MRI," *Science Advances* 7, no. 1 (2021): eabc8180.

52. A. L. Kern, H. Biller, F. Klimeš, et al., "Noninvasive Monitoring of the Response of Human Lungs to Low-Dose Lipopolysaccharide Inhalation Challenge Using Mri: A Feasibility Study," *Journal of Magnetic Resonance Imaging* 51, no. 6 (2020): 1669–1676.

53. D. Xinmin, D. Yunyou, P. Chaosheng, et al., "Dexamethasone Treatment Attenuates Early Seawater Instillation-Induced Acute Lung Injury in Rabbits," *Pharmacological Research* 53, no. 4 (2006): 372–379.

54. F. Terzi, B. Demirci, İ. Çınar, M. Alhilal, and H. S. Erol, "Effects of Tocilizumab and Dexamethasone on the Downregulation of Proinflammatory Cytokines and Upregulation of Antioxidants in the Lungs in Oleic Acid-Induced ARDS," *Respiratory Research* 23, no. 1 (2022): 249.

55. J. Zhang, J. Huo, Z. Zhao, et al., "An Anticomplement Homogeneous Polysaccharide From *Hedyotis diffusa* Attenuates

Lipopolysaccharide-Induced Acute Lung Injury and Inhibits Neutrophil Extracellular Trap Formation," *Phytomedicine* 107 (2022): 154453.

56. T. Dassios, O. Kaltsogianni, A. Hickey, R. Bhat, and A. Greenough, "Chronology and Determinants of Respiratory Function Changes Following Administration of Systemic Postnatal Corticosteroids in Extremely Preterm Infants," *Journal of Pediatrics* 215 (2019): 17–23.

57. G. C. Motta-Ribeiro, T. Winkler, E. L. V. Costa, N. de Prost, M. R. Tucci, and M. F. Vidal Melo, "Worsening of Lung Perfusion to Tissue Density Distributions During Early Acute Lung Injury," *Journal of Applied Physiology* 135, no. 2 (2023): 239–250.

58. L. C. Song, X. X. Chen, J. G. Meng, et al., "Effects of Different Corticosteroid Doses and Durations on Smoke Inhalation-Induced Acute Lung Injury and Pulmonary Fibrosis in the Rat," *International Immunopharmacology* 71 (2019): 392–403.

59. M. J. McIntosh, H. K. Kooner, R. L. Eddy, et al., "Asthma Control, Airway Mucus, and ^{129}Xe MRI Ventilation After a Single Benralizumab Dose," *Chest* 162, no. 3 (2022): 520–533.

60. L. E. Olsson, A. Smailagic, P. O. Onnervik, A. Lindén, and P. D. Hockings, "^{1}H and Hyperpolarized ^{3}He Magnetic Resonance Imaging Clearly Detect the Preventative Effect of a Glucocorticoid on Endotoxin-Induced Pulmonary Inflammation In Vivo," *Innate Immunity* 17, no. 2 (2011): 204–211.

61. H. Guo, R. Yang, J. He, et al., "Edaravone Combined With Dexamethasone Exhibits Synergic Effects on Attenuating Smoke-Induced Inhalation Lung Injury in Rats," *Biomedicine & Pharmacotherapy* 141 (2021): 111894.

62. G. Norquay, G. Leung, N. J. Stewart, J. Wolber, and J. M. Wild, "^{129}Xe Chemical Shift in Human Blood and Pulmonary Blood Oxygenation Measurement in Humans Using Hyperpolarized ^{129}Xe NMR," *Magnetic Resonance in Medicine* 77, no. 4 (2017): 1399–1408.

63. Y. Friedlander, B. Zanette, A. Lindenmaier, et al., "Chemical Shift of ^{129}Xe Dissolved in Red Blood Cells: Application to a Rat Model of Bronchopulmonary Dysplasia," *Magnetic Resonance in Medicine* 84, no. 1 (2020): 52–60.

64. S. Y. Feng, J. Gao, J. Wang, and Y. Li, "Effects of Prolonged Methylprednisolone Treatment After Pulse Therapy for Paraquat-Intoxicated Rats," *Human & Experimental Toxicology* 37, no. 1 (2018): 21–26.

65. D. Teng, Q.-f. Pang, W.-j. Yan, W. Z. Xin, and C.-y. Xu, "The Harmful Effect of Prolonged High-Dose Methylprednisolone in Acute Lung Injury," *International Immunopharmacology* 15, no. 2 (2013): 223–226.

66. A. Kozan, N. Kilic, H. Alacam, A. Guzel, T. Guvenc, and M. Acikgoz, "The Effects of Dexamethasone and L-NAME on Acute Lung Injury in Rats With Lung Contusion," *Inflammation* 39, no. 5 (2016): 1747–1756.

67. D. Mokra, P. Mikolka, P. Kosutova, and J. Mokry, "Corticosteroids in Acute Lung Injury: The Dilemma Continues," *International Journal of Molecular Sciences* 20, no. 19 (2019): 4765–4788.

68. X. Q. Wang, X. Zhou, Y. Zhou, L. Rong, L. Gao, and W. Xu, "Low-Dose Dexamethasone Alleviates Lipopolysaccharide-Induced Acute Lung Injury in Rats and Upregulates Pulmonary Glucocorticoid Receptors," *Respirology* 13, no. 6 (2008): 772–780.

69. F. Amzajerdian, H. Hamedani, R. Baron, et al., "Simultaneous Quantification of Hyperpolarized Xenon-129 Ventilation and Gas Exchange With Multi-Breath Xenon-Polarization Transfer Contrast (XTC) MRI," *Magnetic Resonance in Medicine* 90, no. 6 (2023): 2334–2347.

Supporting Information

Additional supporting information can be found online in the Supporting Information section. **Table S1:** Summary of statistical results for PFTs and ^{129}Xe MR results from control group and DEX group.